

# Journal of Mechanics of Materials and Structures

INFLUENCE OF GEOMETRY ON SEISMIC CAPACITY OF  
CIRCULAR BUTTRESSED ARCHES

Giuseppe Brandonisio and Antonello De Luca

Volume 14, No. 5

December 2019



## INFLUENCE OF GEOMETRY ON SEISMIC CAPACITY OF CIRCULAR BUTTRESSED ARCHES

GIUSEPPE BRANDONISIO AND ANTONELLO DE LUCA

The effect of geometry on the seismic capacity of masonry buttressed arches with circular shape is addressed in this paper. In particular, in the context of the limit analysis approach for masonry structures, a numerical procedure developed by the authors in previous studies is here used to perform an extensive parametric analysis of 320 circular buttressed arches, obtained by varying the geometrical configuration, namely the angle of embrace, the arch thickness and the buttress aspect ratio. The aim of the parametric analysis is studying the effect of both arch configuration (angle of embrace and arch thickness) and buttress geometry (height and width) on the horizontal strength of buttressed arches. To this end, the results of this study are presented in terms of collapse multiplier and failure mechanism aimed to provide reference values to be used for straightforward assessment of the horizontal strength of arched masonry structures, and for checking the results of more complex structural analyses performed by using “advanced” structural engineering software.

### 1. Introduction

A masonry arch is a construction, usually curved, that spans an opening. It is generally built by placing wedge-shaped blocks (the so-called voussoirs) having their narrower ends toward the opening on temporary centering. Arches vary in shape, from those that have little or no curvature to those that are acutely pointed. These structures are very common in historical masonry buildings, as in the cases of triumphal arches in churches, as colonnades at the base of buildings or in internal patios. Traditionally, the determination of suitable structural dimensions of arches has been carried out by experience in the early ages, and in the modern era through the application of equilibrium principles such as thrust lines. More recently, the availability of the newly developed limit analysis (LA) and elasticity theory has provided more refined tools for analysis and verification of masonry arched structures. The first one, in the approach originally proposed by Kooharian [1952] in his milestone paper for the voussoir arches and then formalized and adapted to unreinforced masonry arches by Heyman [1966] in his seminal paper, is considered particularly appealing. Actually, it requires no material characterization, relying only on the activation of kinematic mechanisms, due to the formation of a sufficient number of nondissipative rotational hinges, and on simple variationally written equilibrium equations.

The possibility of using the LA approach, in the form of kinematic theorem, for the seismic analysis of arched structures is also allowed by Italian Technical Codes [NTC 2008; 2018; CM 2009; Linee guida dei Beni Culturali 2010], that point out the importance of the right selection of the collapse mechanisms that can be activated. To this end, the set of potential failure mechanisms can be a priori selected, thanks to the deep knowledge of the collapse modes collected during the post-earthquake reconnaissance activity

---

*Keywords:* masonry buttressed arch, limit analysis, collapse mechanism, seismic capacity, nonlinear programming.

of the past decades by scholars (see [Russo 1918; Doglioni et al. 1994; Decanini et al. 2004; Lagomarsino and Podestà 2004; D’Ayala and Pagnoni 2011; Dizhur et al. 2011; Lagomarsino 2012; Sorrentino et al. 2013; Brandonisio et al. 2013], among others).

In this contest, the collapse behavior of typical URM elements of churches has been studied by the authors in the last 15 years by using the kinematic approach of LA. The aim in this study was to provide simplified closed form expressions for evaluating the horizontal load multiplier of URM masonry arches [De Luca et al. 2004; Brandonisio et al. 2017a; 2017b] and façades [Giordano et al. 2007; Lucibello et al. 2013; Brandonisio et al. 2015].

The LA approach is used to provide simplified “closed form” expressions of the horizontal collapse multiplier, also taking into account the contribution of steel tie rods (see [Brandonisio et al. 2015] for details). The proposed formulations have been used for performing an extensive parametric analysis, with the aim of studying the effect of both geometry and vertical/horizontal loading distributions on the portal horizontal strength. Furthermore, the influence of the steel tie rods has been addressed in order to understand their effectiveness on the portal seismic capacity.

A numerical procedure based on the application of LA approach combined with the nonlinear programming (NLP) technique is proposed in [Brandonisio et al. 2017a] for the assessment of circular buttressed arches loaded by horizontal forces. The automatic procedure is also validated through the comparison with numerical and experimental data retrieved from the literature. The validation result shows the reliability of the proposed procedure both in terms of activated collapsed mode and of actual horizontal load multiplier  $\lambda$ .

The reliability of the proposed procedure has been also assessed in [Brandonisio et al. 2017b] through the comparison with the real response of two triumphal arches of the Santa Maria delle Grazie church in Navelli (AQ) during the 2009 L’Aquila earthquake. The comparison has shown a good agreement in terms of failure mechanism, of hinges positions and of horizontal capacity, showing the reliability of the numerical procedure.

In this paper the numerical procedure is used to perform a wide parametric analysis of 320 circular buttressed arches. The aim was to grasp the influence of the buttressed arch geometry on its horizontal strength by varying the geometrical configuration, i.e., angle of embrace, arch thickness and buttress aspect ratio.

## 2. The masonry buttressed arches

Figure 1 shows a schematic representation of circular buttressed arch with the indication of the main parameters that allows for defining its geometry, namely: the inner radius ( $R$ ), the clear span ( $L$ ), the arch thickness ( $t$ ), the centre height ( $h_0$ ), the angle of embrace ( $2\omega$ ), the buttress height ( $h$ ), the buttress width ( $B$ ), the global width ( $D$ ) and the global height ( $H$ ).

Therefore, the geometry of buttressed arch can be parameterized by adopting appropriate geometrical ratios (appointed as fundamental ratios in the following), that are the arch thickness over radius ratio ( $t/R$ ), the buttress width over radius ratio ( $B/R$ ) and the buttress height over radius ( $h/R$ ). In Figure 1 are also depicted the loads acting on the structure, consisting of gravity loads ( $W$ ) and horizontal actions that increase proportionally to the vertical forces through a horizontal loading multiplier  $\lambda$ .

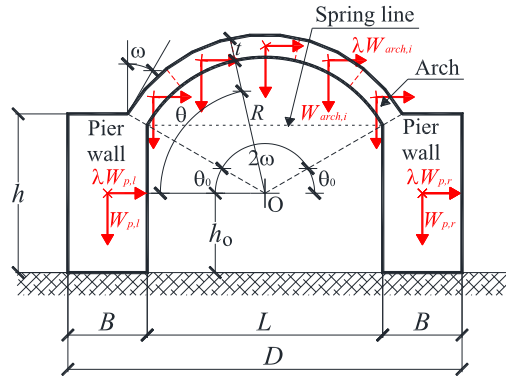


**Figure 1.** Masonry buttressed arch: geometry and loads.

The geometrical dimensions of arches have been established by the experience of ancient builders, on the bases of theory of proportions under the assumption that the static of arches under gravity loads is governed uniquely by their geometry. Therefore, several rules of thumb were used to establish the more appropriate arch geometry, the minimum thickness and the minimum buttress thickness.

With reference to the circular arch shape, the current paper aims to investigate on the seismic capacity of buttressed arches designed according to empirical rules of art. The rules are based on the theory of proportions used in the past for the stability of arched structures under gravity loads (see also [Milani 1923; Benvenuto 1981; 1991; Brandonisio and De Luca 2019]).

### 3. Limit analysis of buttressed arches under horizontal loading through nonlinear programming

A brief description of the numerical procedure proposed by the authors in [Brandonisio et al. 2017a] for the seismic assessment of circular buttressed arches is provided in this section.

The procedure is based on the application of the kinematic theorem of limit analysis approach coupled with the use of NLP technique, and it can be schematized in the following steps:

- (1) identification and analysis of all the potential failure mechanisms that can be activated for the buttressed arch. These mechanisms can be defined on the basis of similar structures damaged during the past earthquakes, or based on the existing crack patterns;
- (2) calculation of horizontal load multiplier  $\lambda$  that causes the activation of each considered collapse mechanism under the well-known Heyman's assumptions on the masonry material (null tensile strength; infinite compression strength; sliding of a stone or of a part of the structure upon another cannot occur);
- (3) evaluation of actual horizontal load multiplier  $\lambda$  as the minimum among the ones calculated for the considered collapse mechanisms.

Concerning the potential failure mechanisms that can be significant for a buttressed arch under seismic actions (step 1), on the basis of considerations provided in [Como 2013] and [Brandonisio et al. 2017a], three failure modes are considered:

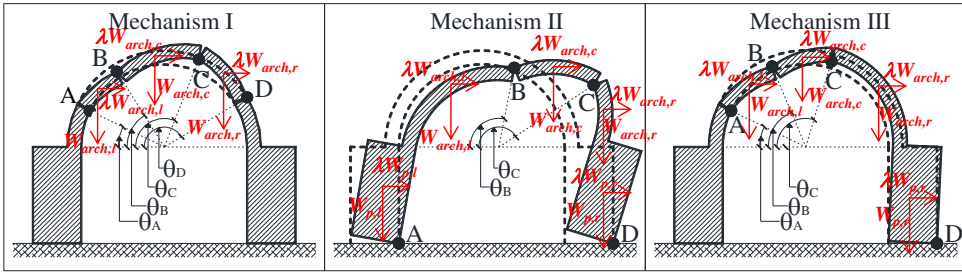


**Figure 2.** Considered collapse mechanisms: arch mechanism (mech. I, left), global mechanism (mech. II, center), and mixed mechanism (mech. III, right).

- (1) arch mechanism (Figure 2, left), also appointed as mechanism I, characterized by the activation of four hinges A, B, C, and D within the development of the arch, whose locations are identified through the angles  $\theta_A$ ,  $\theta_B$ ,  $\theta_C$  and  $\theta_D$ , measured with respect to the horizontal line;
- (2) global mechanism (Figure 2, center), also appointed as mechanism II, that considers the rocking of the two piers about two hinges A and D at the pier basis and two hinges B and C within the arch, whose positions are defined by the angles  $\theta_B$  and  $\theta_C$ , respectively;
- (3) mixed mechanism (Figure 2, right), also appointed as mechanism III, having one hinge D at the base of the pier on the opposite side of the horizontal force and three hinges A, B and C within the development of the arch, whose positions are identified by the angles  $\theta_A$ ,  $\theta_B$  and  $\theta_C$ , respectively.

For each selected collapse mechanisms of Figure 2 (step 2), the horizontal load multiplier can be evaluated by using the kinematic theorem of LA through the application of the principle of virtual works that allows for writing

$$\lambda^j = \frac{W_{p,l} \cdot v_{p,r} + \sum_{i=l,r,l} [W_{arch,i}(\vartheta_k) \cdot v_{arch,i}(\sin(\vartheta_k), \cos(\vartheta_k))] + W_{p,r} \cdot v_{p,r}}{W_{p,l} \cdot u_{p,r} + \sum_{i=l,r,l} [W_{arch,i}(\vartheta_k) \cdot u_{arch,i}(\sin(\vartheta_k), \cos(\vartheta_k))] + W_{p,r} \cdot u_{p,r}}, \quad (1)$$

where  $\lambda^j$  is the horizontal load multiplier, given by the ratio between the horizontal load ( $F^j$ ) that activates the corresponding mechanism  $j$  ( $j = I, II, III$ ) and the total vertical load ( $W_{tot} = W_{p,l} + W_{arch} + W_{p,r}$ );  $W_{p,l}$  and  $W_{p,r}$  are the self-weight of left and right buttress, respectively;  $W_{arch,i}$  ( $i = l, c, r$ ) is the self-weight of three rigid parts of the arch ( $l = \text{left}, c = \text{central}, r = \text{right}$ ) involved in the collapse mechanism that are identified by the angles  $\theta_i$  ( $i = A, B, C, D$ ) that define the position of the hinges in the arch (therefore, the weight of the whole arch is:  $W_{arch} = W_{arch,l} + W_{arch,c} + W_{arch,r}$ );  $v_{p,i}$  and  $u_{p,i}$  ( $i = l, r$ ) are the vertical and horizontal displacements of the centroid of the pier walls ( $l = \text{left}, r = \text{right}$ );  $v_{arch,i}$  and  $u_{arch,i}$  ( $i = l, c, r$ ) are the vertical and horizontal displacements of the centroid of the three parts of the arch ( $l = \text{left}, c = \text{central}, r = \text{right}$ ) involved in the collapse mechanism.

The expressions for evaluating the weights and the displacement components of the rigid bodies involved in the kinematical chains are reported in [Brandonisio et al. 2017a].

Finally (step 3), the actual horizontal load multiplier  $\lambda$  is evaluated as the minimum value among the three multipliers  $\lambda^I$ ,  $\lambda^{II}$ ,  $\lambda^{III}$  that have to be calculated according to the equation (1):

$$\lambda = \min \begin{cases} \lambda_{\min}^I = \min[\lambda^I(\vartheta_A, \vartheta_B, \vartheta_C, \vartheta_D)] \\ \lambda_{\min}^{II} = \min[\lambda^{II}(\vartheta_B, \vartheta_C)] \\ \lambda_{\min}^{III} = \min[\lambda^{III}(\vartheta_A, \vartheta_B, \vartheta_C)], \end{cases} \quad (2)$$

To this end, nonlinear optimization techniques, based on the Generalized Reduced Gradient (GRG) code as implemented in [Lasdon et al. 1978], is used since the parameters involved in (1) for the evaluation of the horizontal load multipliers  $\lambda^j$  have nonlinear relationship with the hinge locations. In fact, as specified in [Brandonisio et al. 2017a], the weights  $W_{\text{arch},l}$ ,  $W_{\text{arch},c}$ ,  $W_{\text{arch},r}$  are function of the angles  $\theta_k$  and the components of displacements of the rigid blocks formed in the arch vary with  $\sin \theta_k$  and  $\cos \theta_k$ , where  $j = I, II, III$  and  $k = A, B, C, D$ .

Therefore, the application of nonlinear optimization problem to the three failure mechanisms of Figure 2, allows for obtaining the position of the hinges in the arch, through the value of the angles  $\theta_A$ ,  $\theta_B$ ,  $\theta_C$  and  $\theta_D$  (nonnegative unknown variables) that minimizes the objective function  $\lambda^j = \lambda^j(\theta_A, \theta_B, \theta_C, \theta_D)$  given by (1).

The constraint conditions that define the nonlinear optimization problem (i.e., the boundary conditions that the unknown variables  $\theta_i$  ( $i = A, B, C, D$ ) have to satisfy for each failure mechanism of Figure 2) are imposed by assuming that the first hinge in the arch can occur at a minimum inclination of  $\theta_0 = \pi/2 - \omega$  with respect to the springing line (i.e.,  $\theta_{A,\min} = \theta_0$  for the mechanisms I and III;  $\theta_{B,\min} = \theta_0$  for the mechanism II), while the last hinge was considered with a maximum inclination of  $\pi - \theta_0$  with respect to the springing line (i.e.,  $\theta_{D,\min} = \pi - \theta_0$  for the mechanism I;  $\theta_{C,\min} = \pi - \theta_0$  for the mechanisms II and III).

#### 4. Parametric analysis of circular buttressed arches: description of 320 case studies, activated collapse mechanisms and seismic capacity

**4.1. Description of 320 case studies.** The numerical procedure illustrated in the previous section for evaluating the seismic capacity of masonry buttressed arches is herein parametrically applied on 320 case studies obtained by varying the main geometrical parameters that define the arch configuration.

In detail, the analyzed buttressed arches have been obtained by varying the following geometrical parameters:

- angle of embrace  $2\omega$ , according to four configurations of the arch depression, i.e.,  $2\omega = 90^\circ, 120^\circ, 150^\circ, 180^\circ$ ;
- arch thickness  $t$ , variable in the range:  $t/R = 0.10, 0.20, 0.30, 0.40$ ;
- buttress height  $h$ , variable between one and four times the inner radius of the arch  $R$ , i.e.,  $h/R = 1.00, 2.00, 3.00, 4.00$ ;
- buttress width  $B$ , variable between 38% and 125% of the arch  $R$ , namely:  $B/R = 0.38, 0.50, 0.75, 1.00, 1.25$ .

As underlined in [Brandonisio and De Luca 2019], the stepwise variability of the fundamental ratios used in the parametric analysis allows for covering the geometry of masonry arches built according to the rules of thumb.

The combination of the values fixed for the fundamental ratios allows for obtaining 320 different geometries, whose seismic analyses give us a proper understanding of the effect of geometry on the horizontal strength of buttressed arches. In order to better explain this concept, Figure 3 shows an abacus with the geometry of some analyzed structures; the red arrows underline the influence of the investigated parameters, namely: (i) the angle of embrace  $2\omega$ , whose effect can be appreciated by looking at the horizontal red arrow provided at the bottom of the figure that goes from depressed arches on the left side (corresponding to  $2\omega = 90^\circ$ ) to semicircular arches on the right side (corresponding to  $2\omega = 180^\circ$ ); (ii) the arch thickness  $t/R$ , whose influence can be studied, for a fixed value of the angle of embrace  $2\omega$ , by looking at the horizontal red arrows at the top of Figure 3; (iii) the buttress slenderness, that varies with the  $h/R$  ratio, as outlined by the vertical short arrows; (iv) the buttress width, represented by the  $B/R$  ratio, whose influence is remarked by the vertical arrow provided on the left side of the abacus of Figure 3.

The geometrical representation of the 320 examined buttressed arches is provided in figures 4 and 5 that have been divided in macrorows, each two corresponding to a fixed value of the arch thickness  $t/R$ , and in four macrocolumns, each column corresponding to a fixed value of the buttress width  $B/R$ . Every framework defined by a couple of  $t/R$  and  $B/R$  ratios has been again subdivided into 16 squares corresponding to the four fixed values of angle of embrace  $2\omega$  and to the four fixed values of the  $h/R$  ratio.

Depending on the arch thickness-to-radius ratio, the overall view of the 320 buttressed arches in figures 4 and 5 allows for classifying the arches in: (i) thin arches, when  $t/R = 0.10$  (see the left side of Figure 4); (ii) arches with medium thickness, namely  $t/R = 0.20$  and  $t/R = 0.30$ , as depicted on the right side of Figure 4 and on the left side of Figure 5, respectively; and (iii) thick arches, when  $t/R = 0.40$  (see the right side of Figure 5). This classification in thin, medium and thick arches will be useful in the next subsections for discussing the results of parametric analysis in terms of activated collapse mechanism and of seismic capacity.

**4.2. Prevailing collapse mechanisms.** Figure 6 shows a synoptic framework of the activated collapse mechanisms resulting from the parametric analysis. By looking at the figure it is possible to understand when one failure mechanism prevails on another depending on the buttressed arch geometry.

According to the format used in figures 4 and 5, Figure 6 is composed by four frames, each one corresponding to a value of the arch thickness  $t/R$ . Every frame is divided in four columns corresponding to the investigated values of angle of embrace  $2\omega$ , and in five macrorows, each two corresponding to a fixed value of the buttress width  $B/R$ , that in turn are subdivided in four lines associated to the stepwise variability of the  $h/R$  ratio. The arched structures collapsed according to the arch mechanism have been depicted by using a grey square appointed with the Roman numeral “I” to indicate the mechanism I; similarly, the global and the mixed failure modes have been plotted with green and white squares appointed with the Roman numeral “II” and “III” to mean the activation of the mechanism II or of the mechanism III, respectively.

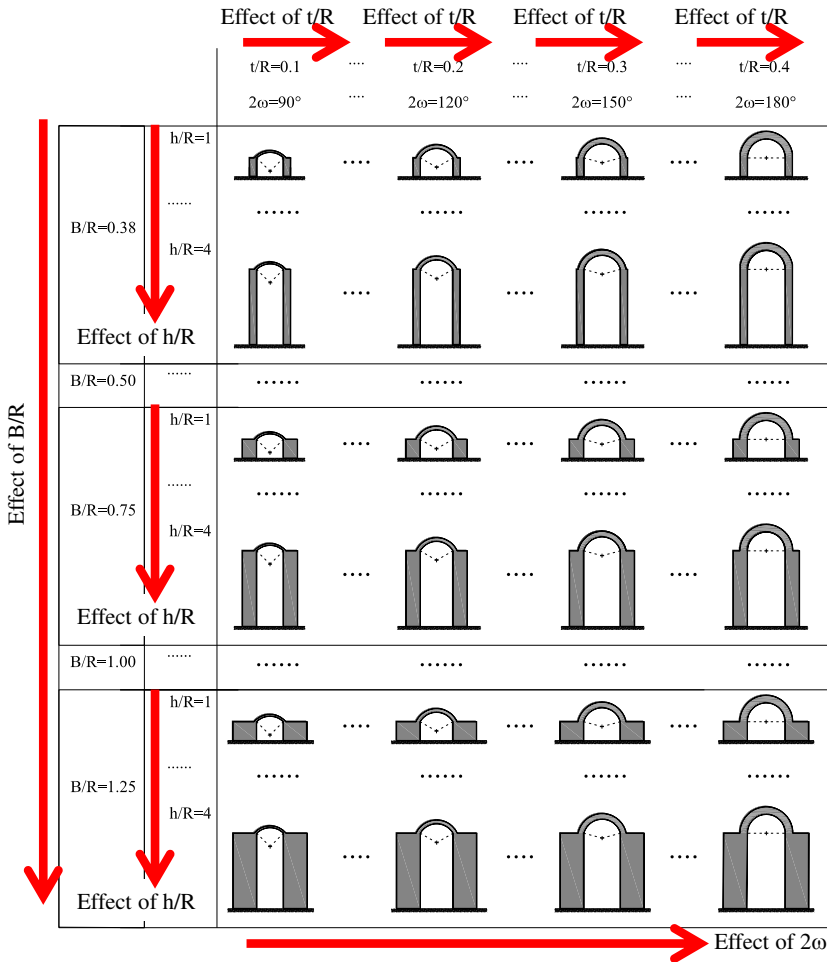


**Figure 3.** Analyzed geometric parameters of buttressed arches: effect of fundamental ratios  $h/R$ ,  $B/R$ ,  $t/R$  and  $2\omega$ .

From the synoptic framework (Figure 6), it can be observed that the prevailing failure modes are the mixed (or mech. III) and, in minor recurrence, the arch mechanisms (or mech. I). In fact, the global mechanism II occurs only in two semicircular buttressed arches with  $t/R = 0.40$  and  $h/R = 1$ .

The mixed mechanism is always activated in presence of depressed arches (i.e.,  $2\omega = 90^\circ$ ), and it generally prevails in presence of buttressed arches characterized by angle of embrace equal to  $2\omega = 150^\circ$  and  $2\omega = 120^\circ$ .

On the contrary, the arch mechanism I prevails in presence of semicircular buttressed arches ( $2\omega = 180^\circ$ ), as well as in the cases for arches with medium thickness and stocky buttresses, when the angle of embrace is equal to  $2\omega = 150^\circ$  and  $2\omega = 120^\circ$ .

Finally, from the synoptic framework of Figure 6 it can be observed that semicircular buttressed arches with thin thickness (i.e.,  $t/R = 0.10$ ) have no lateral capacity because the arch thickness is not able to contain the thrust line modified by the presence of horizontal forces.





**Figure 4.** Geometry of analyzed buttressed arches: thin arch thickness,  $t/R = 0.10$  (left column) and medium arch thickness,  $t/R = 0.20$  (right column).

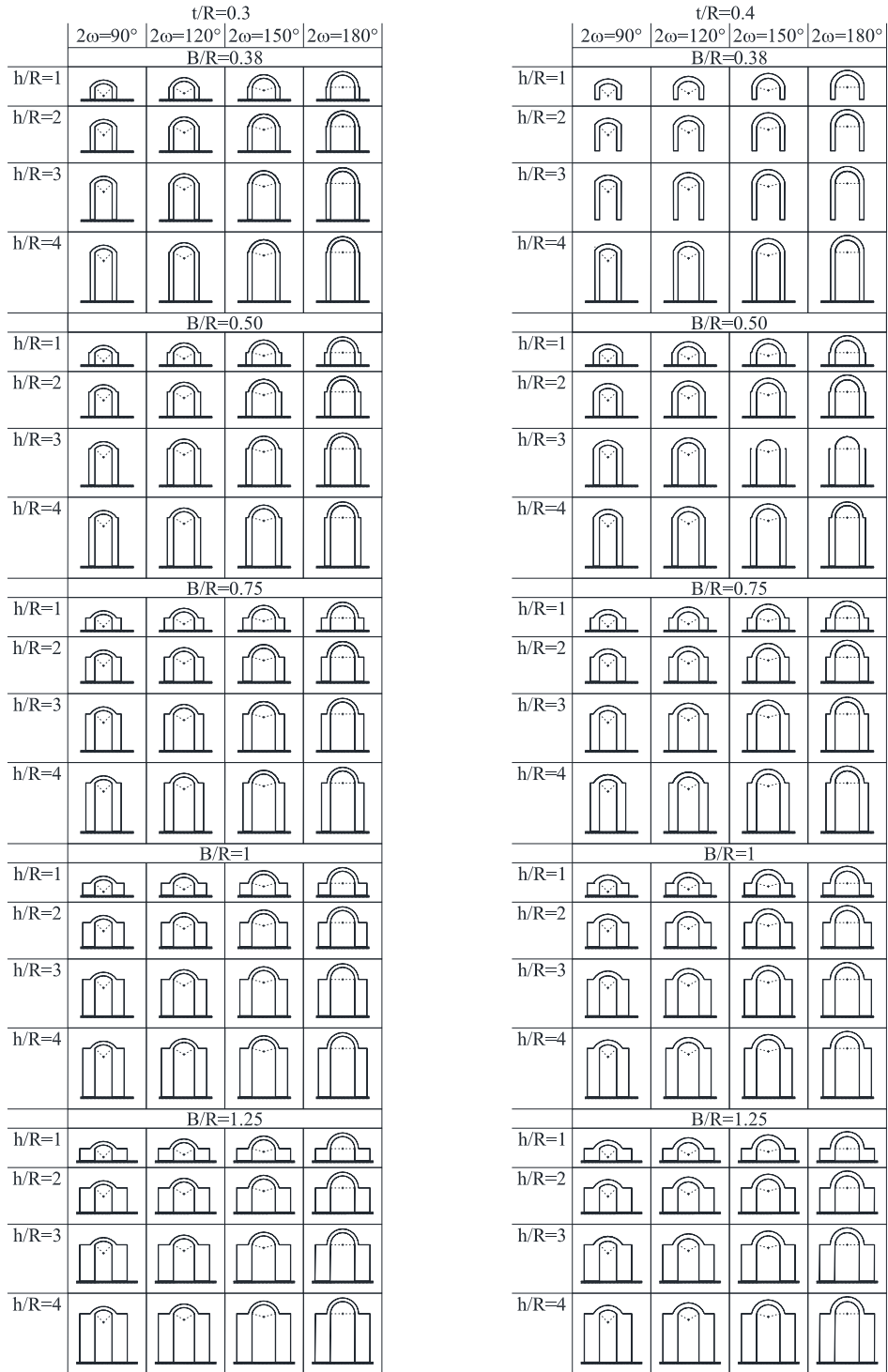


**Figure 5.** Geometry of analyzed buttressed arches: medium arch thickness,  $t/R = 0.30$  (left column) and thick arch thickness,  $t/R = 0.40$  (right column).

		t/R=0.10 (Thin arch thickness)					t/R=0.20 (Medium arch thickness)			
		2ω=90°	2ω=120°	2ω=150°	2ω=180°		2ω=90°	2ω=120°	2ω=150°	2ω=180°
B/R=0.38	h/R=1	III	III	III	No horizontal capacity	III	III	III	I	
	h/R=2	III	III	III		III	III	III	I	
	h/R=3	III	III	III		III	III	III	I	
	h/R=4	III	III	III		III	III	III	I	
B/R=0.5	h/R=1	III	III	III		III	III	III	I	
	h/R=2	III	III	III		III	III	III	I	
	h/R=3	III	III	III		III	III	III	I	
	h/R=4	III	III	III		III	III	III	I	
B/R=0.75	h/R=1	III	III	I		III	III	III	I	
	h/R=2	III	III	I		III	III	III	I	
	h/R=3	III	III	I		III	III	III	I	
	h/R=4	III	III	I		III	III	III	I	
B/R=1	h/R=1	III	I	I		III	III	I	I	
	h/R=2	III	I	I		III	III	I	I	
	h/R=3	III	III	I		III	III	III	I	
	h/R=4	III	III	I		III	III	III	I	
B/R=1.25	h/R=1	III	I	I	III	I	I	I		
	h/R=2	III	I	I	III	I	I	I		
	h/R=3	III	I	I	III	III	I	I		
	h/R=4	III	I	I	III	III	I	I		

		t/R=0.30 (Medium arch thickness)				t/R=0.40 (Thick arch thickness)			
		2ω=90°	2ω=120°	2ω=150°	2ω=180°	2ω=90°	2ω=120°	2ω=150°	2ω=180°
B/R=0.38	h/R=1	III	III	III	I	III	III	III	III
	h/R=2	III	III	III	III	III	III	III	III
	h/R=3	III	III	III	III	III	III	III	III
	h/R=4	III	III	III	III	III	III	III	III
B/R=0.5	h/R=1	III	III	III	I	III	III	III	I
	h/R=2	III	III	III	I	III	III	III	III
	h/R=3	III	III	III	I	III	III	III	III
	h/R=4	III	III	III	III	III	III	III	III
B/R=0.75	h/R=1	III	III	III	I	III	III	III	II
	h/R=2	III	III	III	I	III	III	III	I
	h/R=3	III	III	III	I	III	III	III	I
	h/R=4	III	III	III	I	III	III	III	I
B/R=1	h/R=1	III	III	I	I	III	III	III	II
	h/R=2	III	III	I	I	III	III	III	I
	h/R=3	III	III	III	I	III	III	III	I
	h/R=4	III	III	III	I	III	III	III	I
B/R=1.25	h/R=1	III	III	I	I	III	III	III	I
	h/R=2	III	III	I	I	III	III	III	I
	h/R=3	III	III	I	I	III	III	III	I
	h/R=4	III	III	I	I	III	III	III	I

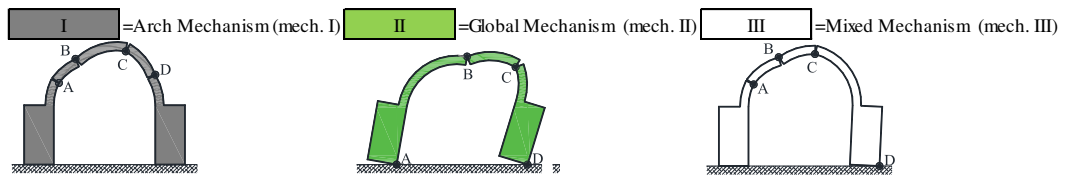


Figure 6. Activated collapse mechanisms.

**4.3. Seismic capacity.** The results of the parametric analysis are summarised in figures 7 and 8 in terms of horizontal load multiplier  $\lambda$  and angle of embrace  $2\omega$  curves. In detail, the diagrams of Figure 7 (left column) refer to the thin arch thickness ( $t/R = 0.10$ ), the diagrams of Figure 7 (right column) and of Figure 8 (left column) refer to medium arch thickness (i.e.,  $t/R = 0.20$  and  $t/R = 0.30$ , respectively), while the diagrams of Figure 8 (right column) are related to the arches with thick thickness ( $t/R = 0.40$ ).

The five diagrams of each column refer to the fixed values of the  $B/R$  ratio, namely  $B/R = 0.38, 0.50, 0.75, 1.00, 1.25$ , while the four curves plotted in each diagram correspond to the investigated values of the  $h/R$  ratio (i.e.,  $h/R = 1, 2, 3, 4$ ).

The overall vision of the diagrams of figures 7 and 8 allows for observing a different trend of the  $\lambda(2\omega, h/R)$  curves, depending on the  $t/R$  ratio. In fact, in presence of thin arches ( $t/R = 0.10$ ) the  $\lambda(2\omega, h/R)$  curves of Figure 7 (left column) have a decreasing trend with the angle of embrace. Otherwise, in presence of medium arch thickness the diagrams of Figure 7 (right column) and of Figure 8 (left column) have a subhorizontal trend and the four curves corresponding to stocky buttresses ( $B/R < 0.75$ ) are superimposed because the horizontal strengths of these case studies are slightly afflicted by the  $h/R$  ratio. Finally, in the cases of thick arch thickness ( $t/R = 0.40$ ), the curves of Figure 8 (right column) show an increasing trend with  $2\omega$ .

Concerning the seismic capacity of buttressed arches with thin thickness ( $t/R = 0.10$ ), by looking at the diagrams of Figure 7 (left column) it can be firstly observed that the depressed arches have larger horizontal capacities, while the semicircular ones have no horizontal strength. It can be also observed that the  $\lambda(2\omega, h/R)$  curves are horizontal in the depressed arches, and show decreasing evolution with the angle of embrace, where the curves are overlapped due to activation of the arch mechanism that is not affected by the  $t/R$  parameter. Furthermore, it can be noted that the horizontal load multiplier is less than  $\lambda = 20\%$  in presence of angle of embrace  $2\omega \geq 150^\circ$ , while the lateral strength increases up to  $\lambda = 40\%$  to  $60\%$  in the cases of depressed buttressed arches.

Regarding the arched structures with medium thickness ( $t/R = 0.20$  and  $t/R = 0.30$ ), as already observed, the curves have a prevailing horizontal evolution because the lateral capacity is not affected by the angle of embrace. The unique exception is provided by semicircular arches with buttresses characterized by  $t/R = 0.20$ ,  $B/R \geq 1$  and  $h/R \leq 2$  (see Figure 7, right column, fourth and fifth row), where the  $\lambda(2\omega, h/R)$  curves show a decreasing trend induced by the activation of the arch mechanism. Concerning the values of horizontal load multipliers observed in the cases of medium arch thickness, the lateral strength varies with no influence of the  $h/R$  ratio up to  $\lambda = 10\%$  when  $B/R \leq 0.5$ , and in the range  $\lambda = 10\%$  to  $20\%$  when  $B/R = 0.75$ ; in the cases of buttresses with  $B/R \geq 1$ , the load multiplier ranges between  $\lambda = 20\%$  and  $\lambda = 40\%$  and the curves show that the horizontal capacity decreases up to half when the buttress height goes from  $h/R = 1$  to  $h/R = 4$ .

The results obtained from the parametric analysis performed on the structures with thick arch thickness (Figure 8, right column) allows for observation that the horizontal capacity of the buttressed arches characterized by  $B/R \leq 0.5$  is low, being less than  $\lambda = 10\%$  independently by the angle of embrace  $2\omega$  and by the  $h/R$  ratio. In the cases of buttress with  $B/R \geq 0.75$ , it can be noted that the horizontal load multiplier of depressed arches (i.e.,  $2\omega = 90^\circ$  and  $2\omega = 120^\circ$ ) ranging from  $\lambda \cong 10\%$  to  $\lambda \cong 25\%$ , regardless of  $2\omega$  and  $h/R$  parameters; on the contrary, when  $2\omega \geq 150^\circ$ , the  $\lambda(2\omega, h/R)$  curves show an increasing trend and differentiating among them to take into account the value of the  $h/R$  ratio, and the horizontal load multiplier  $\lambda$  rising from  $\lambda = 20\%$  to  $\lambda = 50\%$  passing from  $h/R = 4$  to  $h/R = 1$ .

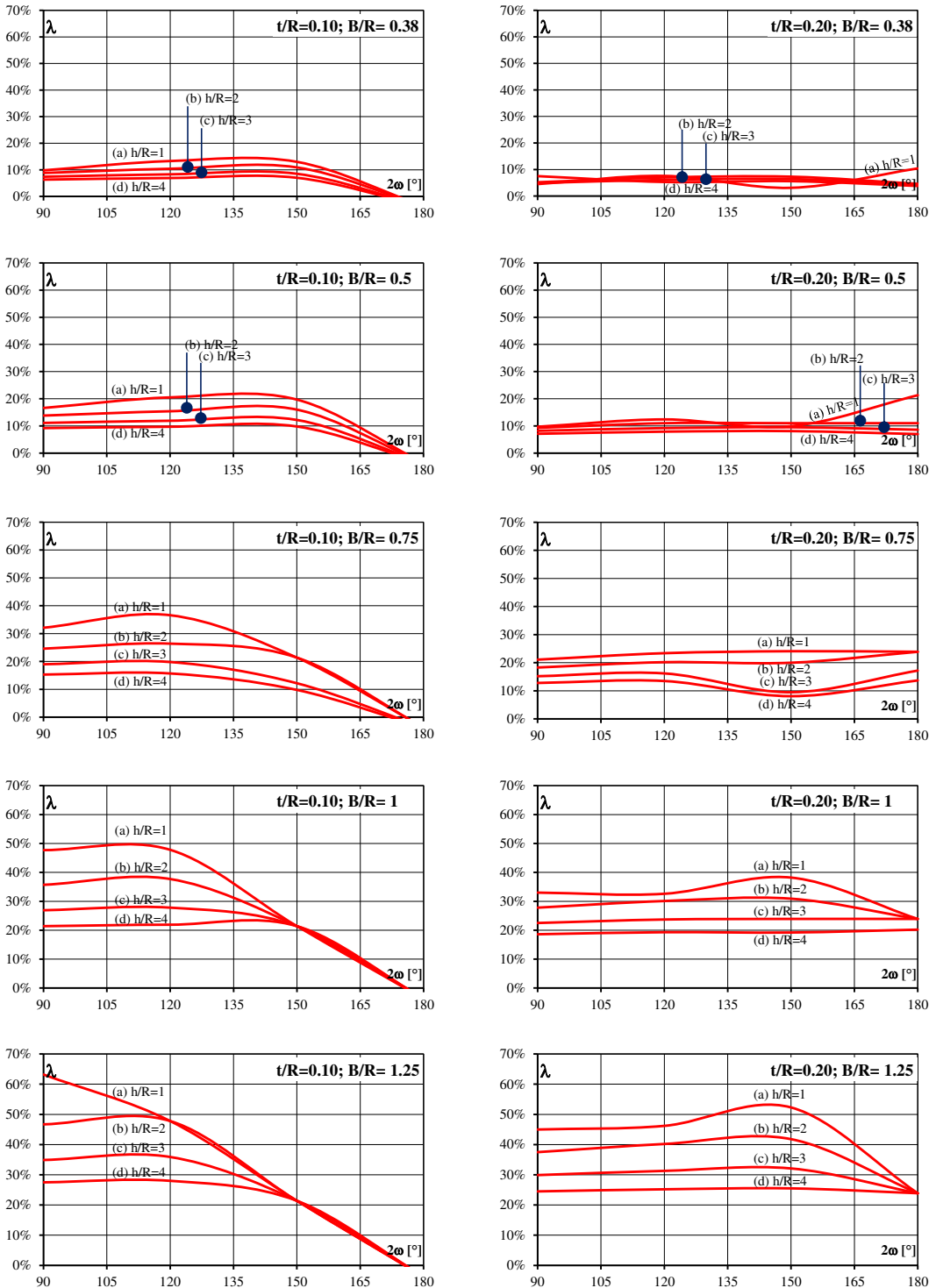


**Figure 7.** Effect of angle of embrace ( $2\omega$ ) on horizontal capacity  $\lambda$  of thin arch thickness ( $t/R = 0.10$ , left column) and medium arch thickness ( $t/R = 0.20$ , right column).

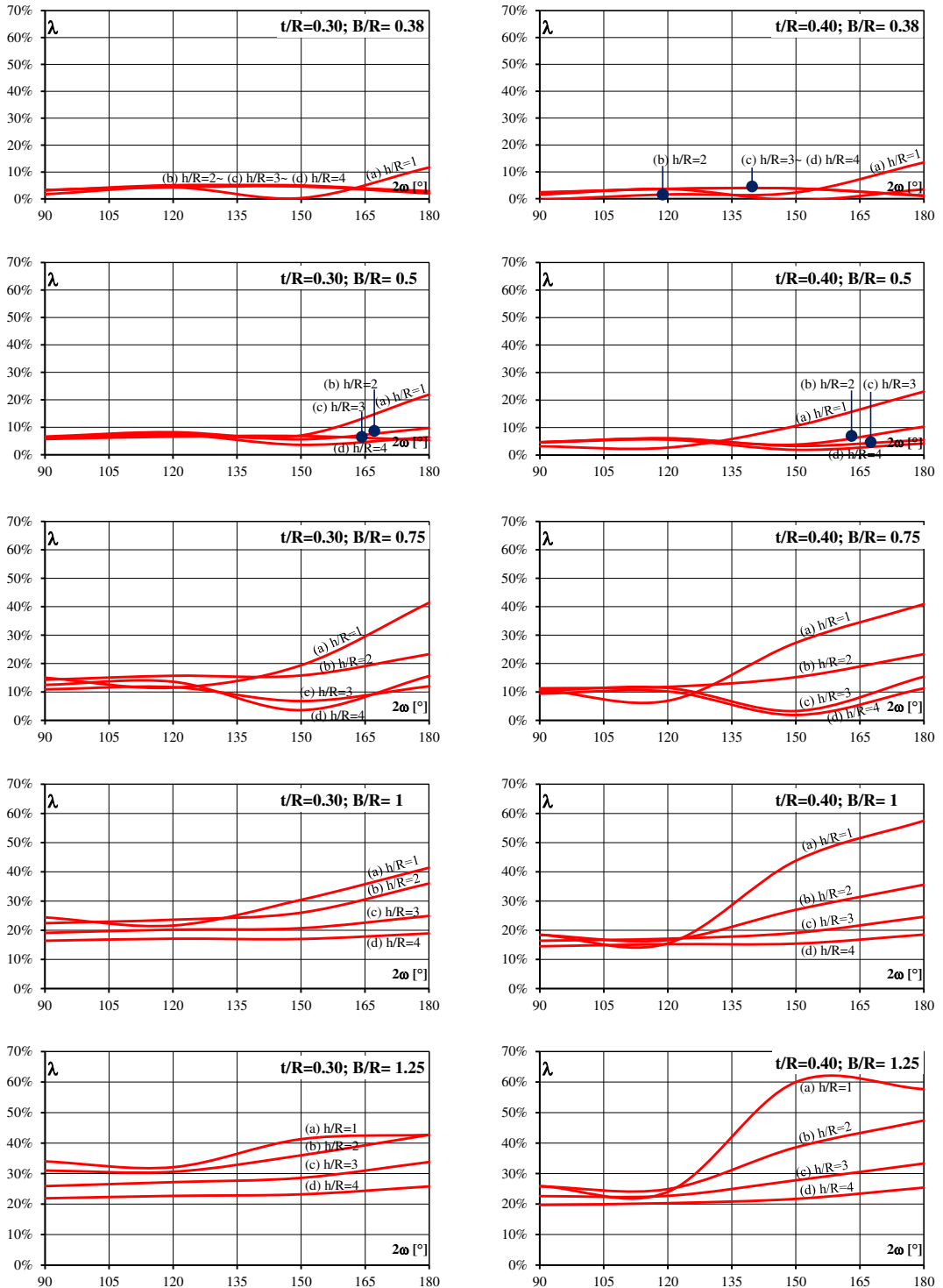


**Figure 8.** Effect of angle of embrace ( $2\omega$ ) on horizontal capacity  $\lambda$  of medium arch thickness ( $t/R = 0.30$ , left column) and thick arch thickness ( $t/R = 0.40$ , right column).

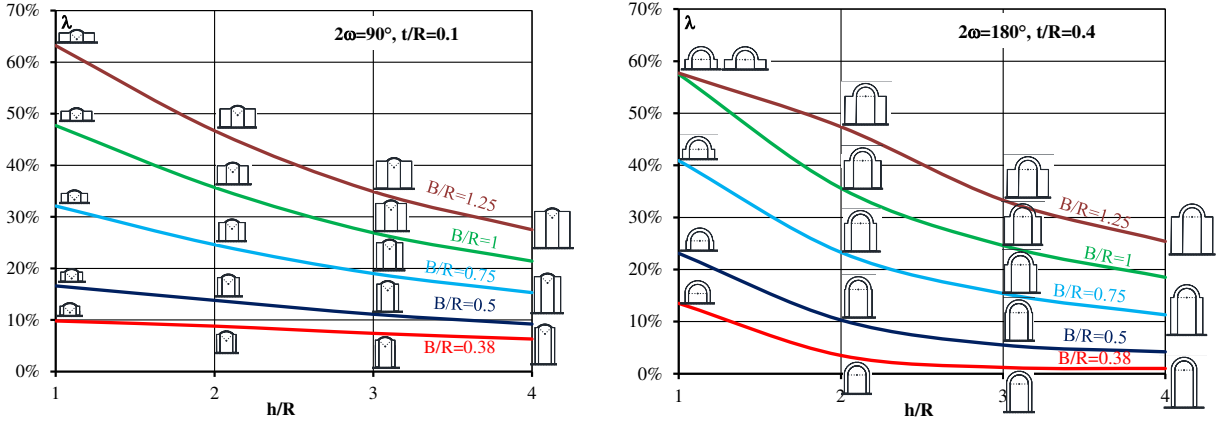


**Figure 9.** Effect of buttress geometry on the horizontal strength of depressed thin arches (left) and on semicircular thick arches (right).

The effect of geometry on the seismic capacity of analyzed buttressed arches can be also established by revising the numerical results according to the format of Figure 9, where the horizontal load multiplier  $\lambda$  has been plotted as a function of the  $h/R$  ratio for the extreme geometrical configuration, namely for depressed arches with thin thickness (i.e.,  $2\omega = 90^\circ$ ,  $t/R = 0.10$  in Figure 9, left) and for semicircular arches with thick thickness (i.e.,  $2\omega = 180^\circ$ ,  $t/R = 0.40$  in Figure 9, right).

Five curves have been plotted in each diagram of Figure 9, each one corresponding to the five investigated values of  $B/R$ . The related geometrical representation of the buttressed arches has been also provided in Figure 9 with the aim of correlating the horizontal capacity with the geometric shape of the examined structures.

Both the diagrams show that the lateral strength  $\lambda$  of buttressed arches decreases from the stockier to the slender buttresses, with higher gradient for semicircular arches that are more sensible to the buttress geometry, i.e., to the  $h/R$  and  $B/R$  ratios, respect to the depressed arches.

These considerations can be extended to all examined case studies by observing the diagrams of Figure 10 that have been plotted by using the same format of Figure 9. In particular, each column in Figure 10 refers to the investigated values of angle of embrace ( $2\omega$ ), while each row concerns to the selected values of nondimensional arch thickness  $t/R$ .

Regarding the buttressed arches with small arch thickness, by looking at the diagrams at the top row of Figure 10 corresponding to  $t/R = 0.10$ , it can be noted how depressed arches ( $2\omega = 90^\circ$ ) have lateral capacity higher than the ones of arched structures with intermediate angles of embrace, namely  $2\omega = 120^\circ$  and  $2\omega = 150^\circ$ , while semicircular arches have no horizontal capacity, as already observed.

Concerning the horizontal capacity of buttressed arches with medium thickness (i.e.,  $t/R = 0.20$  and  $t/R = 0.20$ ), from the second and third rows of Figure 10 it can be observed that the horizontal load multiplier is less affected by the angle of embrace.

On the contrary, in presence of thick arch thickness (see bottom row in Figure 10), it can be noted that the horizontal capacity increases with angle of embrace, showing a more strong dependence by the buttress shape, i.e., by the  $h/R$  and  $B/R$  ratios in presence of arches characterised by  $2\omega = 150^\circ$  and  $2\omega = 180^\circ$ .

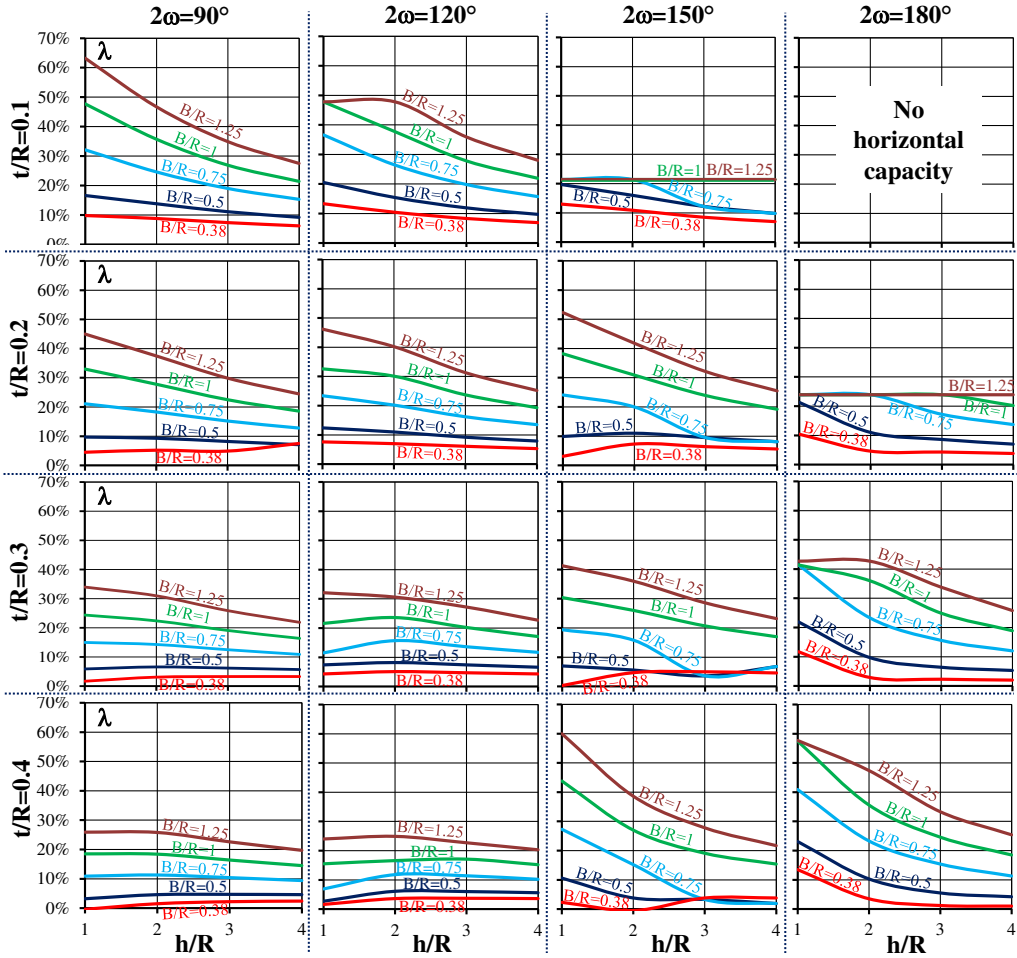


Figure 10. Effect of buttress geometry on the horizontal strength of 320 examined arches.

Finally, it can be observed that the collapse multiplier  $\lambda$  of depressed arches (namely,  $2\omega = 90^\circ$ , left column in Figure 10) strongly decreases with the  $t/R$  ratio, is no longer influenced by the  $t/R$  ratio for arches with angles of embrace  $2\omega = 120^\circ$  and  $2\omega = 150^\circ$ , while, in a different way, the horizontal strength  $\lambda$  of semicircular arches increases greatly with the arch thickness, reaching very high values in presence of thick arch and stocky buttresses, namely  $\lambda = 40\%$  to  $60\%$ .

### 5. Conclusions

In this paper, the effect of geometry on the seismic capacity of masonry buttressed circular arches has been studied in the framework of the limit analysis approach for masonry structures.

The numerical procedure developed by the authors in [Brandonisio et al. 2017a] has been used to perform an extensive parametric analysis of 320 circular buttressed arches, obtained by varying the fundamental ratios that define the arches from a geometrical point of view, namely the angle of embrace ( $2\omega$ ), the arch thickness ( $t/R$ ) and the buttress height ( $t/R$ ) and width ( $B/R$ ).



The results of parametric analysis allowed for establishing that the prevailing failure mechanisms is the “mixed” one, while the “arch” mechanism generally occurs in presence of semicircular arches and of arches characterised by  $2\omega = 150^\circ$  and  $B/R \geq 1$ . The “global” mechanism is activated only in two cases of semicircular arches with thick arch thickness ( $t/R = 0.4$ ) and stocky buttresses.

Concerning the seismic capacity, the numerical analyses discussed in the paper suggests that the horizontal load multiplier  $\lambda$  is very sensitive in presence of depressed and semicircular arch shape (i.e.,  $2\omega = 90^\circ$  and  $2\omega = 180^\circ$ ), while the intermediate configurations of angle of embrace (i.e.,  $2\omega = 120^\circ$  and  $2\omega = 150^\circ$ ) seem to be less influenced by the values of fundamental geometrical ratios.

In particular, the horizontal capacity of depressed arches ( $2\omega = 90^\circ$ ) with thin arch thickness ( $t/R = 0.1$ ), ranging between  $\lambda = 10\%$  and  $\lambda = 60\%$ , is generally 1.5 times to 2 times greater than the capacity of arched structures with both intermediate arch thickness (variable from  $\lambda = 5\%$  to  $\lambda = 40\%$ ) and thick arch thickness (variable between  $\lambda = 5\%$  and  $\lambda = 25\%$ ).

On the contrary, the semicircular arches with the minimum allowable arch thickness (that is  $t/R = 0.1$ ), have no horizontal capacity, that increases in presence of medium thickness, reaching maximum values of seismic capacity equal to  $\lambda = 30\%$  to  $40\%$ . On the contrary, semicircular buttressed arches with thick arch thickness have higher lateral capacity, with horizontal load multipliers that reach values of  $\lambda = 40\%$  to  $50\%$  in presence of stocky buttresses (i.e., when  $h/R \leq 2$  and  $B/R \geq 1$ ).

Finally, buttressed arches with angles of embrace  $2\omega = 120^\circ$  and  $2\omega = 150^\circ$  show intermediate values of seismic capacity, which generally ranges from  $\lambda = 5\%$  to  $\lambda = 40\%$  depending on the buttress geometry.

The authors emphasize the usefulness of the results of parametric analysis provided in this paper, as simple tool for analysts and designers to make a fast evaluation of the seismic capacity of buttressed arches as well as for checking the results of more complex numerical analysis.

### Acknowledgment

This research has been supported by ReLUIS — Research Project 2018 “Rete di Laboratori Universitari Ingegneria Sismica”, in the context of the activities of Task Masonry Structures.

### References

- [Benvenuto 1981] E. Benvenuto, *La scienza delle costruzioni e il suo sviluppo storico*, Sansoni, Firenze, 1981.
- [Benvenuto 1991] E. Benvenuto, *An introduction to the history of structural mechanics — part II: vaulted structures and elastic systems*, Springer, New York, 1991.
- [Brandonisio and De Luca 2019] G. Brandonisio and A. De Luca, “Statics of buttressed masonry arches in light of traditional design rules”, in *AIMETA 2019 — XXIV conference of the Italian Association of Theoretical and Applied Mechanics* (Rome, Italy), 2019.
- [Brandonisio et al. 2013] G. Brandonisio, G. Lucibello, and E. M. A. De Luca, “Damage and performance evaluation of masonry churches in the 2009 L’Aquila earthquake”, *Eng. Fail. Anal.* **34** (2013), 693–714.
- [Brandonisio et al. 2015] G. Brandonisio, E. Mele, and A. De Luca, “Closed form solution for predicting the horizontal capacity of masonry portal frames through limit analysis and comparison with experimental test results”, *Eng. Fail. Anal.* **55** (2015), 246–270.
- [Brandonisio et al. 2017a] G. Brandonisio, E. Mele, and A. De Luca, “Limit analysis of masonry circular buttressed arches under horizontal loads”, *Meccanica (Milano)* **52**:11-12 (2017), 2547–2565.
- [Brandonisio et al. 2017b] G. Brandonisio, E. Mele, and A. De Luca, “Seismic capacity of URM buttressed arches”, pp. 1555–1569 in *Proc. of AIMETA 2017 XXIII conference — the Italian Association of Theoretical and Applied Mechanics*, 2017.

- [CM 2009] CM, *Istruzioni per l'applicazione delle "Norme tecniche per le costruzioni"*, 2009.
- [Como 2013] M. Como, *Statics of historic masonry constructions*, Springer, Berlin Heidelberg, 2013.
- [D'Ayala and Pagnoni 2011] D. F. D'Ayala and S. Pagnoni, "Assessment and analysis of damage in L'Aquila historic city centre after 6th April 2009", *Bull. Earthq. Eng.* **9**:1 (2011), 81–104.
- [De Luca et al. 2004] A. De Luca, A. Giordano, and E. Mele, "A simplified procedure for assessing the seismic capacity of masonry arches", *Eng. Struct.* **26**:13 (2004), 1915–1929.
- [Decanini et al. 2004] L. Decanini, A. De Sortis, A. Goretti, R. Langenbach, F. Mollaioli, and A. Rasulo, "Performance of masonry buildings during the 2002 Piedritise, Italy, Earthquake", *Earthq. Spectra* **20**:S1 (2004), S191–S220.
- [Dizhur et al. 2011] D. Dizhur, J. Ingham, L. Moon, M. Griffith, A. Schultz, I. Senaldi, G. Magenes, J. Dickie, S. Lissel, J. Centano, C. Ventura, J. Leite, and P. Lourenco, "Performance of masonry buildings and churches in the 22 February 2011 Christchurch earthquake", *Bull. New Zealand Soc. Earthq. Eng.* **44**:4 (2011), 279–296.
- [Doglioni et al. 1994] F. Doglioni, A. Moretti, and V. Petrini, *Le chiese e il terremoto. Dalla vulnerabilità constatata nel terremoto del Friuli al miglioramento antisismico nel restauro*, Lint Editoriale, Trieste, 1994.
- [Giordano et al. 2007] A. Giordano, A. De Luca, E. Mele, and A. Romano, "A simple formula for predicting the horizontal capacity of masonry portal frames", *Eng. Struct.* **29**:9 (2007), 2109–2123.
- [Heyman 1966] J. Heyman, "The stone skeleton", *Int. J. Solids Struct.* **2**:2 (1966), 249–279.
- [Kooharian 1952] A. Kooharian, "Limit analysis of voussoir (segmental) and concrete arches", *ACI J.* **49**:12 (1952), 317–328.
- [Lagomarsino 2012] S. Lagomarsino, "Damage assessment of churches after L'Aquila earthquake (2009)", *Bull. Earthq. Eng.* **10**:1 (2012), 73–92.
- [Lagomarsino and Podestà 2004] S. Lagomarsino and S. Podestà, "Seismic vulnerability of ancient churches: II. Statistical analysis of surveyed data and methods for risk analysis", *Earthq. Spectra* **20**:2 (2004), 395–412.
- [Lasdon et al. 1978] L. S. Lasdon, A. D. Waren, A. Jain, and M. Ratner, "Design and testing of a generalized reduced gradient code for nonlinear programming", *ACM Trans. Math. Softw.* **4**:1 (1978), 34–50.
- [Linee guida dei Beni Culturali 2010] Linee guida dei Beni Culturali, "Linee Guida per la valutazione e riduzione del rischio sismico di patrimonio culturale con riferimento alle Norme tecniche per le costruzioni di cui al D.M. 14/01/2008", 2010.
- [Lucibello et al. 2013] G. Lucibello, G. Brandonisio, E. Mele, and A. De Luca, "Seismic damage and performance of Palazzo Centi after L'Aquila earthquake: a paradigmatic case study of effectiveness of mechanical steel ties", *Eng. Fail. Anal.* **34** (2013), 407–430.
- [Milani 1923] G. B. Milani, *L'Ossatura murale — parte II: L'Estetica*, S. Lattes & C. Editori, 1923.
- [NTC 2008] NTC, *Norme Tecniche per le costruzioni*, 2008. S.O. n. 30, G. U. n. 29.
- [NTC 2018] NTC, *Norme Tecniche per le costruzioni*, 2018. S.O. n. 8, G. U. n. 42.
- [Russo 1918] C. Russo, *Trattato sulle lesioni dei fabbricati*, Unione Tipografico-Editrice Torinese, Torino, 1918.
- [Sorrentino et al. 2013] L. Sorrentino, L. Liberatore, L. D. Decanini, and D. Liberatore, "The performance of churches in the 2012 Emilia earthquakes", *Bull. Earthq. Eng.* **12**:5 (2013), 2299–2331.

Received 8 Jun 2018. Revised 14 May 2019. Accepted 19 Aug 2019.

GIUSEPPE BRANDONISIO: [giuseppe.brandonisio@unina.it](mailto:giuseppe.brandonisio@unina.it)  
Department of Structures for Engineering and Architecture (Di.St.), University of Naples "Federico II", P.le Tecchio, 80,  
80125 Naples, Italy

ANTONELLO DE LUCA: [antonio.deluca@unina.it](mailto:antonio.deluca@unina.it)  
Department of Structures for Engineering and Architecture (Di.St.), University of Naples "Federico II", P.le Tecchio, 80,  
80125 Naples, Italy

# JOURNAL OF MECHANICS OF MATERIALS AND STRUCTURES

[msp.org/jomms](http://msp.org/jomms)

Founded by Charles R. Steele and Marie-Louise Steele

## EDITORIAL BOARD

ADAIR R. AGUIAR	University of São Paulo at São Carlos, Brazil
KATIA BERTOLDI	Harvard University, USA
DAVIDE BIGONI	University of Trento, Italy
MAENGHYO CHO	Seoul National University, Korea
HUILING DUAN	Beijing University
YIBIN FU	Keele University, UK
IWONA JASIUK	University of Illinois at Urbana-Champaign, USA
DENNIS KOCHMANN	ETH Zurich
MITSUTOSHI KURODA	Yamagata University, Japan
CHEE W. LIM	City University of Hong Kong
ZISHUN LIU	Xi'an Jiaotong University, China
THOMAS J. PENCE	Michigan State University, USA
GIANNI ROYER-CARFAGNI	Università degli studi di Parma, Italy
DAVID STEIGMANN	University of California at Berkeley, USA
PAUL STEINMANN	Friedrich-Alexander-Universität Erlangen-Nürnberg, Germany
KENJIRO TERADA	Tohoku University, Japan

## ADVISORY BOARD

J. P. CARTER	University of Sydney, Australia
D. H. HODGES	Georgia Institute of Technology, USA
J. HUTCHINSON	Harvard University, USA
D. PAMPLONA	Universidade Católica do Rio de Janeiro, Brazil
M. B. RUBIN	Technion, Haifa, Israel

**PRODUCTION** [production@msp.org](mailto:production@msp.org)

SILVIO LEVY Scientific Editor


Cover photo: Mando Gomez, [www.mandolux.com](http://www.mandolux.com)

See [msp.org/jomms](http://msp.org/jomms) for submission guidelines.

JoMMS (ISSN 1559-3959) at Mathematical Sciences Publishers, 798 Evans Hall #6840, c/o University of California, Berkeley, CA 94720-3840, is published in 10 issues a year. The subscription price for 2019 is US \$635/year for the electronic version, and \$795/year (+\$60, if shipping outside the US) for print and electronic. Subscriptions, requests for back issues, and changes of address should be sent to MSP.

JoMMS peer-review and production is managed by EditFLOW® from Mathematical Sciences Publishers.

PUBLISHED BY

 **mathematical sciences publishers**  
nonprofit scientific publishing

<http://msp.org/>

© 2019 Mathematical Sciences Publishers

<b>Preface</b>	<b>MAURIZIO ANGELILLO and SANTIAGO HUERTA FERNÁNDEZ</b>	<b>601</b>
<b>Studying the dome of Pisa cathedral via a modern reinterpretation of Durand-Claye's method</b>	<b>DANILO AITA, RICCARDO BARSOTTI and STEFANO BENNATI</b>	<b>603</b>
<b>Experimental and numerical study of the dynamic behaviour of masonry circular arches with non-negligible tensile capacity</b>	<b>ALEJANDRA ALBUERNE, ATHANASIOS PAPPAS, MARTIN WILLIAMS and DINA D'AYALA</b>	<b>621</b>
<b>Influence of geometry on seismic capacity of circular buttressed arches</b>	<b>GIUSEPPE BRANDONISIO and ANTONELLO DE LUCA</b>	<b>645</b>
<b>Failure pattern prediction in masonry</b>	<b>GIANMARCO DE FELICE and MARIALAURA MALENA</b>	<b>663</b>
<b>Energy based fracture identification in masonry structures: the case study of the church of "Pietà dei Turchini"</b>	<b>ANTONINO IANNUZZO</b>	<b>683</b>
<b>Displacement capacity of masonry structures under horizontal actions via PRD method</b>	<b>ANTONINO IANNUZZO, CARLO OLIVIERI and ANTONIO FORTUNATO</b>	<b>703</b>
<b>Automatic generation of statically admissible stress fields in masonry vaults</b>	<b>ELENA DE CHIARA, CLAUDIA CENAMO, ANTONIO GESUALDO, ANDREA MONTANINO, CARLO OLIVIERI and ANTONIO FORTUNATO</b>	<b>719</b>
<b>Limit analysis of cloister vaults: the case study of Palazzo Caracciolo di Avellino</b>	<b>ANTONIO GESUALDO, GIUSEPPE BRANDONISIO, ANTONELLO DE LUCA, ANTONINO IANNUZZO, ANDREA MONTANINO and CARLO OLIVIERI</b>	<b>739</b>
<b>The rocking: a resource for the side strength of masonry structures</b>	<b>MARIO COMO</b>	<b>751</b>